DOI: 10.1002/ejic.201001150

Synthesis and Luminescent Properties of Cerium-, Terbium-, or Dysprosium-Doped $Gd_4Si_2O_7N_2$ Materials

Yanhua Song,[a] Ning Guo,[a] and Hongpeng You*[a]

Keywords: Cerium / Terbium / Dysprosium / Luminescence

$Gd_4Si_2O_7N_2$, a new oxynitride, has been prepared and the luminescent properties of the Ce^{3+}, Tb^{3+} or Dy^{3+} doped product have been studied. XRD results indicate that $Gd_4Si_2O_7N_2$ is isostructural with $Tb_4Si_2N_2O_7$ and belongs to the monoclinic system. The SEM image shows that the synthesized powder disperses well and the particle diameter is between 1.40–4.0 μm. Upon excitation at 350 nm, $Gd_4Si_2O_7N_2:Ce^{3+}$ exhibits blue emission peaking at 445 nm, which may have potential application as a blue phosphor in the field of solid state lighting. The major mechanism for the concentration quenching of the Ce^{3+} emission in $Gd_4Si_2O_7N_2:Ce^{3+}$ is dipole-dipole interactions. The emission colour of $Gd_4Si_2O_7N_2:Tb^{3+}$ can be tuned from blue to green by changing the Tb^{3+} concentration. The ratio of yellow to blue emission for $Gd_4Si_2O_7N_2:Dy^{3+}$ grows higher with an increase in the Dy^{3+} concentration. Energy transfer from the Gd^{3+} ions to Tb^{3+} or Dy^{3+} ions in the $Gd_4Si_2O_7N_2$ host was also observed.

Introduction

Rare-earth ion doped phosphors have been playing important roles in modern lighting and display fields because of their abundant emission colours based on $4f \rightarrow 4f$ or $5d \rightarrow 4f$ transitions.[1,2] The Ce^{3+} ion has a $4f^1$ electronic ground state configuration and the luminescence of the Ce^{3+} ion originates from the transition from the lowest 5d level to the ground states. Since the position of the lowest 5d level is strongly influenced by the local coordination, the emission wavelength of Ce^{3+} varies with different host lattices from UV to the visible range and the corresponding emission colours can be tuned from blue to red.[3] Hence, the Ce^{3+} ion is an important activator used in the fields of solid state lighting such as the commercial yellow phosphor $Y_3Al_5O_{12}:Ce^{3+}$(YAG:Ce).[4] Tb^{3+} has an $4f^8$ electronic configuration and shows a strong, well defined green emission due to the $^5D_4 \rightarrow {}^7F_5$ transition and the Tb^{3+} ion has been successfully applied as an activator in many fields.[5–9] The emission of Dy^{3+} is mainly due to transitions of $^4F_{9/2} \rightarrow {}^6H_{15/2}$ in the blue region and $^4F_{9/2} \rightarrow {}^6H_{13/2}$ in the yellow-orange region. Moreover, Dy^{3+} will emit white light at a suitable yellow-to-blue intensity ratio and can be used as single-phased white emitting phosphor for UV-pumped fluorescent lamps and white light-emitting diodes (LEDs).[10]

In recent years, white LEDs have attracted significant attention because they are a new, ultra efficient, low power and environment friendly lighting system.[11] They are supposed to replace traditional incandescent and fluorescent bulbs and are suitable for backlights for portable electronics, medical and automotive applications.[12] The main method to produce white light in LEDs is the phosphor-conversion method and the phosphor most commonly utilised in white LEDs is the yellow-emitting $(Y_{1-a}Gd_a)_3(Al_{1-b}Ga_b)O_{12}:Ce^{3+}$(YAG:Ce). Other types of phosphors such as orthosilicates,[13,14] aluminates[15] and sulfides[16] have also been used in white LEDs.

Besides the traditionally used oxide phosphors, oxynitride/nitride-based phosphors with excellent chemical and thermal stabilities show outstanding luminescence properties such as good quantum efficiency, radiation stability and excellent thermal quenching behaviour.[17] Compared with oxygen, the luminescence of some rare earth ions coordinated with nitrogen appears in the longer-wavelength region owing to the red-shift of energy centre of gravity and the higher formal charge of N^{3-} compared with O^{2-}.[18,19] So a variety of oxynitride and nitride, especially silicon-based nitrides with promising luminescent properties, have been discovered recently. The structures of silicon-based oxynitrides and nitrides are generally built up of networks of crosslinking SiN_4 tetrahedra. This is anticipated to significantly lower the excited state of the 5d electrons of the doped rare-earth elements, due to large crystal-field splitting and a strong nephelauxetic effect. This enables the silicon-based oxynitride and nitride phosphors to have a broad excitation band extending from the ultraviolet to the visible-light range and thus strongly absorb blue-to-green light. The structural versatility of oxynitride and nitride phos-

[a] State Key Laboratory of Rare Earth Resource Utilisation, Changchun Institute of Applied Chemistry, Chinese Academy of Sciences, 130022, P. R. China and Graduate University of the Chinese Academy of Sciences,
Beijing 100049, P. R. China
E-mail: hpyou@ciac.jl.cn

Supporting information for this article is available on the WWW under http://dx.doi.org/10.1002/ejic.201001150.

phors makes it possible to attain all the emission colours of blue, green, yellow and red therefore making them suitable for use in LEDs. The reported oxynitride/nitride phosphors can be divided into three groups: (I) Oxonitridosilicates. The representative phosphors are $MSi_2O_2N_2$ (M = Ca, Sr, Ba):Eu^{2+} (green)[20] and RE-Si-O-N:Ce^{3+}(RE = Y, La) (blue to yellow).[21,22] (II) Nitrides. Prominent examples of such advanced phosphor materials are $Sr_2Si_5N_8$:Eu^{2+} (red),[23,24] $LaSi_3N_5$:Ce^{3+} (blue)[25] and $CaAlSiN_3$:Ce^{3+} (yellow-orange).[26] (III) Oxonitridoaluminosilicates (so-called sialons), obtained by partial substitution of Si by Al and subsequent substitution of N by O. The well-known ones are Ca-α-Sialon:Eu^{2+} ($Ca_{(m/2)-x}Eu_xSi_{12-m-n}Al_{m+n}O_nN_{16-n}$)[27,28] and β-Sialon:$Eu^{2+}$ ($Si_{6-z}Al_zO_zN_{8-z}$, $0 < z \leq 4.2$)[29] which are good yellow-orange and green phosphors. Although many oxynitride phosphors have been reported in the literature, the oxynitride $Gd_4Si_2O_7N_2$ is still missing. Herein we report on the synthesis and crystal structure of Si_3N_4 based oxynitride $Gd_4Si_2O_7N_2$. Furthermore, the luminescence properties of the Ce^{3+}, Tb^{3+} and Dy^{3+} ions have been studied in the obtained $Gd_4Si_2O_7N_2$ matrix.

Results and Discussion

Structure and Morphology of $Gd_4Si_2O_7N_2$

Figure 1 shows the X-ray diffraction patterns of the samples obtained at 1550 °C and the standard curve of $Tb_4Si_2O_7N_2$. On the basis of the Joint Committee on Powder Diffraction Standards (JCPDS) reference database, the patterns could not be indexed exactly to gadolinium compounds. It means that this gadolinium compound has not been reported in the database of JCPDS. A careful analysis found that all diffraction peaks for the sample can be readily indexed to a monoclinic phase of $Tb_4Si_2O_7N_2$ except for a spectral shift toward the smaller angle side, revealing that the obtained precursor is isostructural with the $Tb_4Si_2O_7N_2$ structure. It can be assumed that the obtained samples should have a stoichiometric formula of $Gd_4Si_2O_7N_2$ which is similar to $Tb_4Si_2O_7N_2$. The spectroscopic shift of the diffraction peaks can be explained by the change of ionic radii. When the Tb^{3+} (92.3 pm) ion is substituted by the larger Gd^{3+} (93.8 pm) the *d*-spacing increases and, thus, the diffraction angles decreases accordingly due to Bragg's equation, $2d \sin\theta = \lambda$, where *d* is the distance between two crystal planes, θ is diffraction angle of an observed peak and λ is the X-ray wavelength (0.15405 nm).[30] The cell parameters were calculated by using the Fp-Studio software. The results show that $Gd_4Si_2O_7N_2$ belongs to the monoclinic system, a = 10.7357, b = 10.6032, c = 8.0818, V = 872.26 Å^3, Z = 4. As shown in the inset of Figure 1, the synthesised powder consists of well-dispersed particles with a mean diameter of 1.40–4.0 μm.

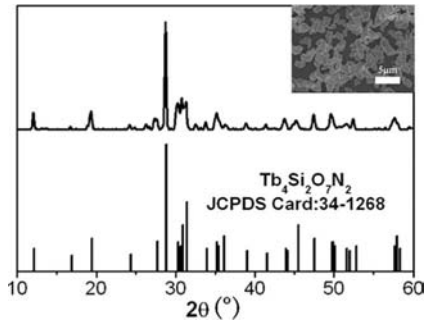

Figure 1. XRD pattern of the $Gd_4Si_2O_7N_2$ sample. The standard data for $Tb_4Si_2O_7N_2$ are shown as references. The inset shows the FESEM micrograph of the sample.

Optical Properties

Luminescence Properties of $Gd_{4-x}Ce_xSi_2O_7N_2$

Figure 2 (a) shows the excitation and emission spectra of the obtained $Gd_{3.98}Ce_{0.02}Si_2O_7N_2$. The excitation band ranges from approximately 200 to 400 nm and shows a strong intensity near 350 nm. This material therefore has a potential application as a UV-excited blue phosphor. The excitation band at 200–250 nm can be attributed to the $Gd_4Si_2O_7N_2$ absorption. The sharp peak at 275 nm originates from the $^8S_{7/2} \rightarrow {}^6I_J$ transition of the Gd^{3+} ions.[31] The broad bands at 290 and 350 nm can be ascribed to the $4f \rightarrow 5d$ transition of the Ce^{3+} ions. Upon excitation at 350 nm, the $Gd_{3.98}Ce_{0.02}Si_2O_7N_2$ phosphor shows a strong broad emission at 445 nm with a full-width half-maximum (FWHM) of 83 nm which is attributed to the $4f5d^1 \rightarrow 4f^1$ transition of the Ce^{3+} ions. The doublet bands due to the transition of the Ce^{3+} ions from the 5d excited state to the $^2F_{5/2}$ and $^2F_{7/2}$ ground states cannot be distinguished directly. However, the emission band can be resolved into two well-separated Gaussian components with maxima at 22938 and 20855 cm^{-1} on an energy scale with an energy difference of about 2083 cm^{-1} (Figure 2, b), which is in agreement with the theoretical difference between the $^2F_{5/2}$ and $^2F_{7/2}$ levels (ca. 2000 cm^{-1}). The dependence of the emission intensity of $Gd_{4-x}Ce_xSi_2O_7N_2$ on the Ce^{3+} concentration is shown in Figure 3 (a). The emission intensity increases with the Ce concentration increasing until a maximum intensity is reached before decreasing due to the concentration quenching. From Figure 3, $Gd_{4-x}Ce_xSi_2O_7N_2$ phosphor samples show maximum emission intensity when the amount of Ce^{3+} is 0.4 mol.-%. The decay curves for the Ce^{3+} (445 nm) can be approximately fitted into a single exponential function as $I = I_0 \exp(-t/\tau)$, in which τ is the decay lifetime (see Supporting Information, Figure S1). The lifetimes of the $Gd_{4-x}Ce_xSi_2O_7N_2$ samples were measured to be 21.35, 21.11, 19.03, 18.68 and 18.35 ns with x = 0.004, 0.005, 0.007, 0.008 and 0.01, respectively. The shortening of the lifetime with the increasing of the Ce^{3+} concentration is due to the concentration quenching.

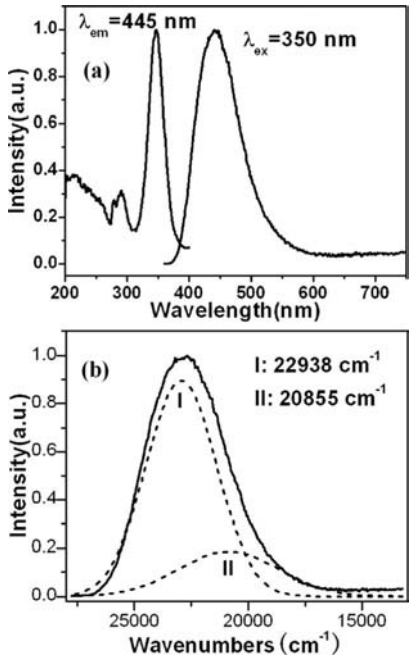

Figure 2. (a) The excitation and emission spectra of $Gd_4Si_2O_7N_2:Ce^{3+}$. (b) The emission spectrum of $Gd_4Si_2O_7N_2:Ce^{3+}$ and the two Gaussian components on an energy scale.

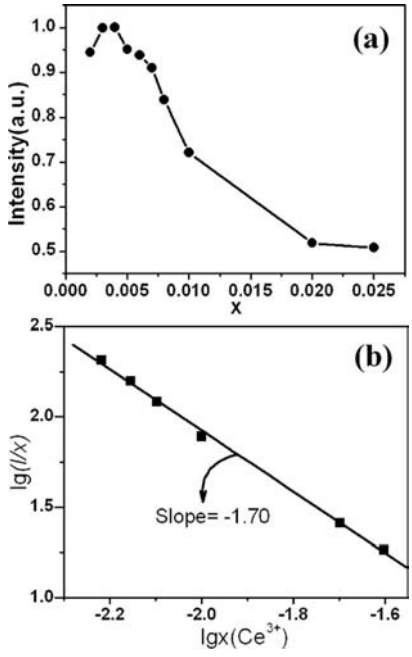

Figure 3. (a) The dependency of emission intensity with various Ce^{3+} concentrations. (b) The curve of $\log I/\chi_{Ce^{3+}}$ vs. $\log\chi_{Ce^{3+}}$ in $Gd_4Si_2O_7N_2:Ce^{3+}$ phosphor (λ_{ex} = 350 nm).

The critical quenching concentration of Ce (χ_c) is defined as the concentration at which the emission intensity begins to decrease and the critical distance is defined as the average distance between the nearest Ce^{3+} ions in which energy transfer occurs. In many cases, concentration quenching is due to the energy transfer from one activator to another until the energy sink in the lattice is reached.[32] Blasse[33] has pointed out that the critical transfer distance (R_c) can be estimated from Equation (1).

$$R_c \approx 2\left(\frac{3V}{4\pi\chi_c N}\right)^{1/3} \quad (1)$$

In this equation V is the volume of the unit cell, N is the number of the host cations in the unit cell and χ_c is the critical concentration of the Ce^{3+} ions. For the $Gd_4Si_2O_7N_2$ host, N is 16 and V is estimated to be 872.26 Å^3. The critical transfer distance of the Ce^{3+} centres in $Gd_4Si_2O_7N_2:Ce^{3+}$ is calculated to be 29.6 Å. Nonradiative energy transfer between different Ce^{3+} ions may occur by exchange interactions or multipole-multipole interactions. The exchange interactions are generally responsible for the energy transfer of forbidden transitions and the typical critical distance is about 5 Å.[34] This indicates that the mechanism of exchange interactions plays little role in the energy transfer between Ce^{3+} ions in this phosphor. The fluorescence mechanism of the Ce^{3+} ions in $Gd_4Si_2O_7N_2$ phosphor is the allowed 5d-4f electric-dipole transition so the process of the energy transfer should be controlled by electric multipole-multipole interactions according to Dexter's theory.[26] If the energy transfer occurs between the same sorts of activators, the intensity of multipolar interactions can be determined from the change of the emission intensity from the emitting level which has the multipolar interactions. The emission intensity (I) per activator ion follows Equation (2).[35,36]

$$I/x = K\left[1+\beta(\chi)^{Q/3}\right]^{-1} \quad (2)$$

In this equation χ is the activator concentration, Q = 6, 8 or 10 for dipole–dipole, dipole–quadrupole or quadrupole–quadrupole interaction, respectively, and K and β are constants for the same excitation condition for a given host crystal. Figure 3 (b) shows that the dependence of $\log(I/\chi_{Ce^{3+}})$ on $\log(\chi_{Ce^{3+}})$ is linear and the slope is –1.70. The value of Q can be calculated as 5.10, which is approximately equal to 6. This indicates that the dipole–dipole interaction is the major mechanism for concentration quenching of the central Ce^{3+} emission in $Gd_4Si_2O_7N_2:Ce^{3+}$.

Luminescence Properties of $Gd_{4-x}Tb_xSi_2O_7N_2$

The excitation spectrum of $Gd_4Si_2O_7N_2:Tb^{3+}$ is shown in Figure 4(a). It exhibits an intense band at 265 nm which is due to the host absorption and the transitions from the ground state ($^7F_6$) of the Tb^{3+} $4f^8$ configuration to the different excited states of the $4f^75d$ configuration. The sharp peaks at 275 and 313 nm derive from the $^8S_{7/2}\rightarrow{}^6I_J$ and $^8S_{7/2}\rightarrow{}^6P_J$ transitions of the Gd^{3+} ions, revealing that an energy transfer from Gd^{3+} to Tb^{3+} ions occurs. The forbidden f-f excited transitions of the Tb^{3+} ions can not be observed and this is clearly due to their weak intensity com-

pared to that of the allowed $4f^8$–$4f^75d$ transition. A similar broadband in the UV part of the spectrum has also been observed for Tb^{3+} in other systems.[19,37] The position of the excitation band is at a relatively low energy which is similar to that of the Tb^{3+} ions in the nitrogen-rich environment.[19] The position of the excitation band matches very well with the 254 nm radiation which may apply in the field of mercury discharge lighting. The emission spectra of $Gd_{4-x}Tb_xSi_2O_7N_2$ samples, obtained by excitation at 254 nm, are shown in Figure 4 (b). It is obvious that the spectroscopic energy distribution of the Tb^{3+} emission depends strongly on the Tb^{3+} concentration. The emission spectra show different ratios between the $^5D_3$ and the $^5D_4$ emissions at lower and higher Tb^{3+} concentrations. The emission spectrum at low Tb^{3+} concentrations consists of the transitions from both the $^5D_3$ and $^5D_4$ levels. For Tb^{3+} ions, the energy gap between the $^5D_3$ and $^5D_4$ levels is close to that between the $^7F_6$ and $^7F_0$ levels. With an increase in the Tb^{3+} concentration, the emissions from the $^5D_3$ to the ^7F_J levels are quenched gradually by the cross-relaxation process between neighbouring Tb^{3+} ions[38]:

$$Tb^{3+}(^5D_3) + Tb^{3+}(^7F_6) \rightarrow Tb^{3+}(^5D_4) + Tb^{3+}(^7F_0)$$

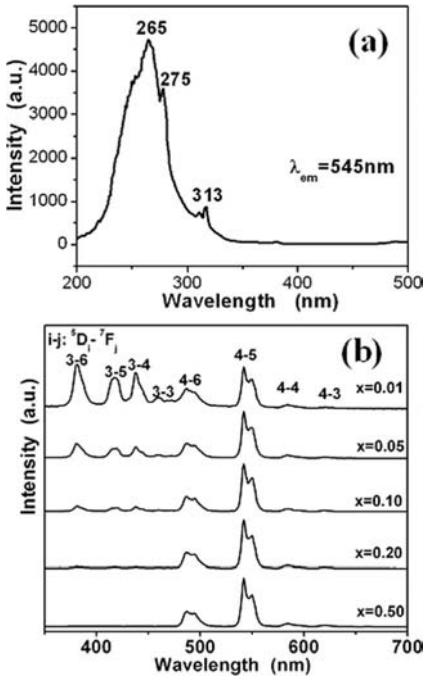

Figure 4. (a) The excitation spectrum of $Gd_4Si_2O_7N_2$:Tb^{3+}. (b) The emission spectra of $Gd_{4-x}Tb_xSi_2O_7N_2$ (λ_{ex} = 254 nm).

Thus the emission spectrum of $Gd_{3.80}Tb_{0.20}Si_2N_2O_7$ shows four peaks at 486, 545, 583 and 620 nm which can be assigned to the $^5D_4$ to ^7F_J (J = 6, 5, 4, 3) transitions, respectively. Among them, the green emission of the $^5D_4 \rightarrow {}^7F_5$ transition at 545 nm is clearly predominant at the higher Tb^{3+} concentration. The decay curve of $Gd_{3.95}Tb_{0.05}Si_2O_7N_2$ can be approximately fitted into a single exponential function as $I = I_0\exp(-t/\tau)$ in which τ is the decay lifetime. The lifetime of the Tb^{3+} ($^5D_4$ level) ions was determined to be 1.1 ms (see Supporting Information, Figure S1). The Commission Internationale de L'Eclairage (CIE) chromaticity coordinates for $Gd_{4-x}Tb_xSi_2O_7N_2$ excited at 254 nm have been calculated (see Supporting Information, Figure S2). With increasing Tb^{3+} content, the chromaticity coordinates (x, y) vary systematically from (0.212, 0.275) to (0.266, 0.588) with a corresponding gradual colour tone change in the samples from blue to green.

Luminescence Properties of $Gd_{4-x}Dy_xSi_2O_7N_2$

Figure 5 shows the excitation and emission spectra of the $Gd_4Si_2O_7N_2$:Dy^{3+} samples. The excitation spectrum monitored at 576 nm for the emission of the Dy^{3+} ($^4F_{9/2} \rightarrow {}^6H_{13/2}$) consists of a strong excitation band from 200 to 300 nm with a maximum at 254 nm and some weak lines (275, 313, 354, 367, 389, 427, 456 and 478 nm) in the longer wavelength region. The broad band is derived from the host absorption, indicating that there is an energy transfer from the host absorption to the Dy^{3+} ions. The lines at 275 and 313 nm can be attributed to the $^8S_{7/2} \rightarrow {}^6I_J$ and $^8S_{7/2} \rightarrow {}^6P_J$ transitions of the Gd^{3+} ions. The appearance of the absorptions of the Gd^{3+} ions in the excitation spectrum confirm an energy transfer from Gd^{3+} to Dy^{3+} ions. The others are due to the f-f transitions ($^6H_{15/2} \rightarrow {}^6P_{7/2}$, $^6H_{15/2} \rightarrow {}^6P_{5/2}$, $^6H_{15/2} \rightarrow {}^6M_{21/2}$, $^6H_{15/2} \rightarrow {}^6G_{11/2}$, $^6H_{15/2} \rightarrow {}^6I_{15/2}$ and $^6H_{15/2} \rightarrow {}^4F_{9/2}$) of the Dy^{3+} ions within its $4f^9$ configuration.[39] Upon UV excitation at 254 nm, the emission spectrum of the $Gd_4Si_2O_7N_2$:Dy^{3+} consists of characteristic emission lines of the Dy^{3+} ions at 486, 576 and 672 nm which can be attributed to the $^4F_{9/2} \rightarrow {}^6H_{15/2}$, $^4F_{9/2} \rightarrow {}^6H_{13/2}$ and $^4F_{9/2} \rightarrow {}^6H_{11/2}$ transitions, respectively. The effect of the Dy^{3+} concentration on the emission has also been investigated. Both emission bands increase with the increasing Dy^{3+} concentration up to 2.5 mol-% (Figure 6). In general, the luminescence branching ratio is a critical parameter because it characterises the possibility of attaining stimulated emission from any specific transition. Branching ratios for yellow and blue originating from $^4F_{9/2}$ were evaluated experimentally by calculating the integrals under the respective emission bands. Figure 5 (b) shows the emission spectra of the $Gd_{4-x}Dy_xSi_2O_7N_2$ with different Dy^{3+} concentrations. The Y/B ratios of the $Gd_{4-x}Dy_xSi_2O_7N_2$ were calculated to be 0.78, 0.83, 0.85, 1.14, 1.30 and 1.41 with x = 0.01, 0.02, 0.03, 0.04, 0.05 and 0.10, respectively. The data show that the ratio of Y/B becomes higher with the increase in the Dy^{3+} concentration, indicating that the yellow emission becomes stronger than blue emission. The increasing of the luminescence intensity ratios (Y/B) may be attributed to two causes. The main reason is the energy-reabsorption. When the electrons of Dy^{3+} ions are excited from the ground state to the excited state by UV light, these electrons relax to the lowest excited state $^4F_{9/2}$ through multiphonon relaxation then returnto the ground state to produce the Dy^{3+} emissions ($^4F_{9/2} \rightarrow {}^6H_{15/2}$, $^6H_{13/2}$). As shown in Figure 5 (a), there is an absorption peak between 470 and 500 nm in the excitation spectrum for the Dy^{3+} ion. As the concentration of Dy^{3+} ions increases, the distance between

Dy^{3+} ions becomes shorter, so the energy resulting from the $^4F_{9/2} \rightarrow {}^6H_{15/2}$ (486 nm) transition can be reabsorbed and then reemitted from $^4F_{9/2}$ to $^6H_{13/2}$ (576 nm). Hence the blue emission becomes weaker and the yellow emission becomes stronger. The other reason is matrix symmetry. It is known that Dy^{3+} emission around 486 nm ($^4F_{9/2} \rightarrow {}^6H_{15/2}$) is a magnetic dipole transition and that at 576 nm ($^4F_{9/2} \rightarrow {}^6H_{13/2}$) is an electric dipole transition. The $^4F_{9/2} \rightarrow {}^6H_{13/2}$ transition is predominant only when Dy^{3+} ions are located at low-symmetry sites with no inversion centres. As the doping concentration of Dy^{3+} ions increases, there will be a slight deviation from the symmetry in this matrix because of the ionic radii difference between the Gd^{3+} (93.8 Å) and Dy^{3+} (90.8 Å) ions. Hence, the yellow emission becomes stronger than the blue emission and the emission colour can be tuned from blue-white to yellow-white by controlling the Dy^{3+} concentration. The CIE chromaticity coordinates for the $Gd_{4-x}Dy_xSi_2O_7N_2$ have been calculated (Supporting Information, Figure S3). With increasing Dy^{3+} content, the chromaticity coordinates (x, y) vary systematically from (0.348, 0.368) to (0.390, 0.411). The corresponding emission colour can be tuned from white to yellow. The lifetimes of the $Gd_{4-x}Dy_xSi_2O_7N_2$ samples were also measured as 0.404, 0.393, 0.383, 0.378, 0.375, 0.313 and 0.232 ms with x = 0.01, 0.015, 0.02, 0.025, 0.03, 0.05 and 0.10, respectively. The reduction of the lifetime with increasing Dy^{3+} concentration is due to concentration quenching of Dy^{3+} ions.[40] Ningthoujam[41] has reported that the data for the samples with Dy^{3+} concentrations below 15 at.-% were not fitted with a monoexponential decay but, rather, they can be fitted well with a biexponential decay. To understand the behaviour of luminescence decay, we have tried to fit the decay curve of $Gd_{3.975}Dy_{0.025}Si_2O_7N_2$ both with a monoexponential and a biexponential decay equation. The correlation coefficients are 0.8981 and 0.9583, so the decay tendency may be more consistent with the biexponential decay equation (see Supporting Information, Figure S1).

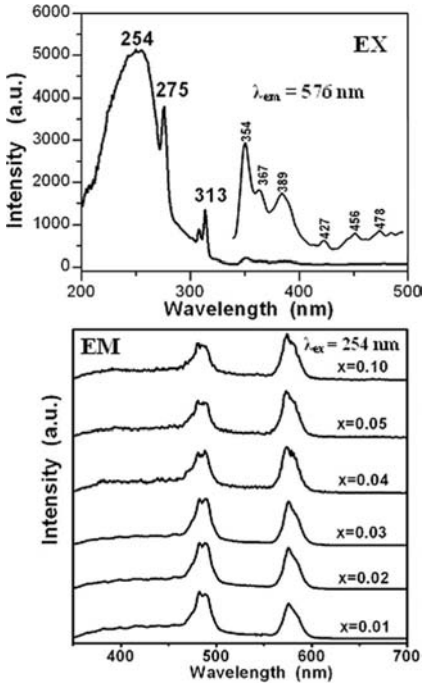

Figure 5. Excitation and emission spectra of $Gd_{4-x}Dy_xSi_2O_7N_2$.

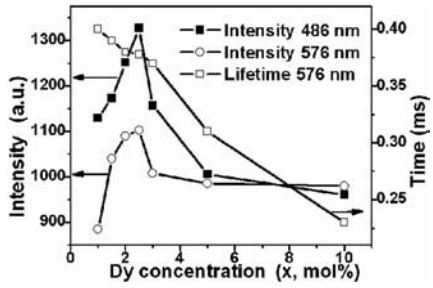

Figure 6. The dependency of emission intensity and lifetime for $Gd_{4-x}Dy_xSi_2O_7N_2$ on the Dy^{3+} concentration.

Conclusions

The $Gd_4Si_2O_7N_2$ material, prepared by a solid state reaction at 1550 °C under a nitrogen atmosphere, is isostructural with $Tb_4Si_2O_7N_2$ and belongs to the monoclinic system. The cell parameters are a = 10.7357, b = 10.6032, c = 8.0818, V = 872.26 Å^3 and Z = 4. Upon excitation at 350 nm, $Gd_4Si_2O_7N_2$:Ce^{3+} phosphor emits blue light peaking at 445 nm which may have a potential application as a blue component in the UV-pumped white LEDs. Upon excitation at 254 nm, the emission colour of $Gd_4Si_2O_7N_2$:Tb^{3+} phosphor can be tuned from blue to green based on the concentration of the Tb^{3+} ions, due to the cross-relaxation process: $Tb^{3+}(^5D_3) + Tb^{3+}(^7F_6) \rightarrow Tb^{3+}(^5D_4) + Tb^{3+}(^7F_0)$. The emission colour of $Gd_4Si_2O_7N_2$:Dy^{3+} phosphor also can be tuned from white to yellow by changing the concentration of Dy^{3+} ions. The energy transfer from the host absorption or Gd^{3+} ions to the Tb^{3+} or Dy^{3+} ions was also observed.

Experimental Section

Sample Preparation: All powder samples of undoped and Ln^{3+}-doped $Gd_4Si_2O_7N_2$ (Ln = Ce, Tb, Dy) were prepared by a solid state reaction at high temperatures. The starting materials were Gd_2O_3 (99.99%), CeO_2 (99.99%), Tb_4O_7 (99.99%), Dy_2O_3 (99.99%) and β-Si_3N_4 (99%). Appropriate amounts of the starting materials were homogeneously mixed in an agate mortar. Subsequently, the powder mixtures were fired in alumina crucibles at 1550 °C for 3 h under a reducing atmosphere of N_2/H_2 (10%) in a horizontal tube furnace. After firing, the samples were cooled to room temperature in the furnace and were ground again with an agate mortar for further measurements.

Characterisation: Powder X-ray diffraction (XRD) measurements were performed on a Bruker D8 focus X-ray powder diffractometer with Cu-K_α radiation (λ = 0.15405 nm). The size and morphology of the samples were inspected using a field emission scanning electron microscopy (FE-SEM, S-4800, Hitachi, Japan). Photoluminescence (PL) excitation and emission spectra were recorded with a

Hitachi F-4500 spectrophotometer equipped with a 150 W xenon lamp as the excitation source. The luminescence decay curves were obtained from a Lecroy Wave Runner 6100 Digital Oscilloscope (1 GHz) using a tuneable laser (pulse width = 4 ns, gate = 50 ns) as the excitation (Contimuum Sunlite OPO). All the measurements were performed at room temperature.

Supporting Information (see footnote on the first page of this article): Luminescence decay curves for $Gd_{3.996}Ce_{0.004}Si_2O_7N_2$, $Gd_{3.80}Tb_{0.20}Si_2O_7N_2$, and $Gd_{3.975}Dy_{0.025}Si_2O_7N_2$; CIE chromaticity diagrams for $Gd_{4-x}Tb_xSi_2O_7N_2$ and $Gd_{4-x}Dy_xSi_2O_7N_2$.

Acknowledgments

This work is financially supported by the National Natural Science Foundation of China (NSFC) Fund for Creative Research Groups (grant number 20921002), and the National Basic Research Program of China (973 Program, grant number 2007CB935502).

[1] G. Blasse, B. C. Grabmaier, *Luminescent Materials*, Springer, Berlin, **1994**.
[2] Y. S. Tang, S. F. Hu, C. C. Lin, N. C. Bagkar, R. S. Liu, *Appl. Phys. Lett.* **2007**, *90*, 151108.
[3] Y. Q. Li, G. de With, H. T. Hintzen, *J. Mater. Chem.* **2005**, *15*, 4492–4496.
[4] D. Jia, Y. Wang, X. Guo, K. Li, Y. K. Zou, W. Jia, *J. Electrochem. Soc.* **2007**, *154*, J1–J4.
[5] M. Z. Su, J. Zhou, K. S. Shao, *J. Alloys Compd.* **1994**, *207*, 406–408.
[6] C. Stoffers, R. Y. Lee, J. Penczek, B. K. Wagner, C. J. Summers, *Appl. Phys. Lett.* **2000**, *76*, 949–951.
[7] Y. C. Kang, I. W. Lenggoro, S. B. Park, K. Okuyama, *J. Phys. Chem. Solids* **1999**, *60*, 1855–1858.
[8] J. A. Kaliakatsos, G. E. Giakoumakis, G. J. Papaioannou, *Solid State Commun.* **1988**, *65*, 35–36.
[9] K. Y. Jung, E. J. Kim, Y. C. Yang, *J. Electrochem. Soc.* **2004**, *151*, H69–H73.
[10] P. Li, Z. Yang, Z. Wang, Q. Guo, *Mater. Lett.* **2008**, *62*, 1455–1457.
[11] S. Nakamura, G. Fasol, *The Blue Laser Diode: GaN-Based Light Emitters and Lasers*, Springer, Berlin, **1997**).
[12] R.-J. Xie, N. Hirosaki, M. Mitomo, *J. Electroceram.* **2007**, *21*, 370–373.
[13] H. S. Jang, D. Y. Jeon, *Appl. Phys. Lett.* **2007**, *90*, 041906–041908.
[14] J. K. Park, M. A. Lim, C. H. Kim, H. D. Park, J. T. Park, S. Y. Choi, *Appl. Phys. Lett.* **2003**, *82*, 683–685.
[15] W. B. Im, N. N. Fellows, S. P. Denbaars, R. Seshadri, Y. I. Kim, *Chem. Mater.* **2009**, *21*, 2957–2966.
[16] D. Jia, D. N. Hunter, *J. Appl. Phys.* **2006**, *100*, 113125.
[17] M. Zeuner, P. J. Schmidt, W. Schnick, *Chem. Mater.* **2009**, *21*, 2467–2473.
[18] H. Yang, Y. Liu, S. Ye, J. Qiu, *Chem. Phys. Lett.* **2008**, *451*, 218–221.
[19] J. W. van Krevel, H. J. W. T. van Rutten, H. Mandal, H. T. Hintzen, R. Metselaar, *J. Solid State Chem.* **2002**, *165*, 19.
[20] Y. Q. Li, A. C. Delsing, G. D. With, H. T. Hintzen, *Chem. Mater.* **2005**, *17*, 3242–3248.
[21] J. W. H. van Krevel, H. T. Hintzen, R. Metselaar, A. Meijerink, *J. Alloys Compd.* **1998**, *268*, 272–277.
[22] B. Dierre, R. J. Xie, N. Nirosaki, *J. Mater. Res.* **2007**, *22*, 1933–1941.
[23] M. Zeuner, P. J. Schmidt, W. Schnick, *Chem. Mater.* **2009**, *21*, 2467.
[24] Y. Q. Li, G. de With, H. T. Hintzen, *J. Lumin.* **2006**, *116*, 107–116.
[25] L. Y. Cai, X. D. Wei, H. Li, Q. L. Liu, *J. Lumin.* **2009**, *129*, 165–168.
[26] Y. Q. Li, N. Hirosaki, R. J. Xie, T. Takeda, M. Mitomo, *Chem. Mater.* **2008**, *20*, 6704–6714.
[27] R. J. Xie, N. Hirosaki, K. Sakuma, Y. Yamamoto, M. Mitomo, *Appl. Phys. Lett.* **2004**, *84*, 5404–5406.
[28] R. J. Xie, N. Hirosaki, M. Mitomo, K. Sakuma, N. Kimura, *Appl. Phys. Lett.* **2006**, *89*, 241103.
[29] K. Kimoto, R. J. Xie, Y. Matsui, K. Ishizuka, N. Hirosaki, *Appl. Phys. Lett.* **2009**, *94*, 041908–041910.
[30] G. Jia, Y. Zheng, K. Liu, Y. Song, H. You, H. Zhang, *J. Phys. Chem. C* **2009**, *113*, 153–158.
[31] J. Zhong, H. Liang, H. Lin, B. Han, Q. Su, G. Zhang, *J. Mater. Chem.* **2007**, *17*, 4679–4684; R. T. Wegh, H. Donker, K. D. Oskam, A. Meijerink, *Science* **1999**, *283*, 663–666.
[32] N. Guo, Y. Song, H. You, G. Jia, M. Yang, K. Liu, Y. Zheng, Y. Huang, H. Zhang, *Eur. J. Inorg. Chem.* **2010**, *29*, 4636–4642.
[33] G. Blasse, *Philips Res. Rep.* **1969**, *24*, 131; M. F. Hazenkamp, G. Blasse, *Chem. Mater.* **1990**, *2*, 105–110.
[34] D. L. Dexter, *J. Chem. Phys.* **1953**, *21*, 836–850.
[35] L. G. Van Uitert, *J. Electrochem. Soc.* **1967**, *114*, 1048.
[36] L. Ozawa, P. M. Jaffe, *J. Electrochem. Soc.* **1971**, *118*, 1678.
[37] H. Jeong, S. Y. Seo, J. H. Shin, *Appl. Phys. Lett.* **2006**, *88*, 161910.
[38] M. Yang, H. You, Y. Song, Y. Huang, G. Jia, K. Liu, Y. Zheng, L. Zhang, H. Zhang, *J. Phys. Chem. C* **2009**, *113*, 20173–20177.
[39] Z. Xiu, Z. Yang, M. Lü, S. Liu, H. Zhang, G. Zhou, *Opt. Mater.* **2006**, *29*, 431.
[40] Y. C. Li, Y. H. Chang, Y. S. Chang, Y. J. Lin, C. H. Laing, *J. Phys. Chem. C* **2007**, *111*, 10682–10688; J. Pisarska, *J. Phys. Condens. Matter* **2009**, *21*, 285101.
[41] N. Shanta Singh, R. S. Ningthoujam, N. Yaiphaba, S. Dorendrajit Singh, R. K. Vatsa, *J. Appl. Phys.* **2009**, *105*, 064303.

Received: October 28, 2010
Published Online: April 4, 2011

